Geobiology

WILEY

gebiology

ORIGINAL ARTICLE OPEN ACCESS

Experimental Mineralisation of a Filamentous Hydrogenotrophic Methanogen in Carbonate, Phosphate, and Silicate

Sigrid Huld[1] | Sean McMahon[2] | Sebastian Willman[1] | Anna Neubeck[1]

[1]Department of Earth Sciences, Uppsala University, Uppsala, Sweden | [2]UK Centre for Astrobiology, School of Physics and Astronomy, University of Edinburgh, James Clerk Maxwell Building, Edinburgh, UK

Correspondence: Sigrid Huld (sigrid.huld@geo.uu.se)

Received: 11 November 2024 | **Revised:** 4 February 2025 | **Accepted:** 10 February 2025

Funding: This study was funded by the Helge Ax: son Johnson Foundation Grant No. F21-0040 and the Swedish Research Council 05018. The Royal Society of Edinburgh #1918.

Keywords: carbonate | experimental mineralisation | methanogens | phosphate | silicate

ABSTRACT

Methanogenic archaea were likely among the earliest organisms to populate the Earth, perhaps contributing to the Archaean greenhouse effect; they are also widely discussed as analogues to any potential life on Mars. However, fossil evidence of archaea has been difficult to identify in the rock record, perhaps because their preservation potential is intrinsically low or because they are particularly small and difficult to identify. Here, we examined the preservation potential of a methanogen of the genus *Methanobacterium*, recently isolated from a low-temperature serpentinizing system, an environment somewhat analogous to habitats on the early Earth and Mars. Notably, this organism has a cell wall composed of peptidoglycan-like pseudomurein, which may imply a mineralisation potential similar to that of gram-positive bacteria. *Methanobacterium* cells were placed in carbonate, phosphate, and silicate solutions for up to 3 months in order to assess the relative tendency of these minerals to encrust and preserve cellular morphology. Cells readily acquired a thick, uniform coating of silica, enhancing their potential for long-term preservation while also increasing overall filament size, an effect that may aid the discovery of fossil archaea while hindering their interpretation. Phosphates precipitated from the medium in all experimental setups and even in parallel experiments set up with low-phosphate medium, suggesting a hitherto unknown biomineralisation capacity of methanogens. Carbonate precipitates did not form in close association with cells.

1 | Introduction

Mineralisation is an important step for fossilising microorganisms at a cellular level with a high degree of fidelity. Rapid entombment of microbes in minerals is often essential for their long-term preservation since it hinders decay and oxidation of the organic matter and can also protect against compaction, mechanical destruction, and molecular degradation (Li et al. 2013; Alleon et al. 2016). This may occur in pores or fractures bearing mineral-supersaturated fluids, particularly around hydrothermal systems, or through biomineralisation (Li et al. 2013). The mineralisation processes of microbes have previously been studied in both modern environments like hot springs and through experimental taphonomy in the laboratory. Experiments are very useful for increasing our understanding of the mechanisms by which the mineralisation of organic structures can occur. Early taphonomic experiments on microbes were performed using cyanobacteria (Oehler and Schopf 1971; Oehler 1976). Since then, a whole host of microbes have been subjected to experimental mineralisation, such as

gram-negative bacteria including iron oxidisers, gram-positive bacteria including *Bacillus subtilis*, thermophilic bacteria, and archaea (Ferris et al. 1988; Westall 1997; Lalonde et al. 2005; Schieber et al. 2008; Orange et al. 2009, 2011; Kish et al. 2016). Mineralisation has been observed to be localised to outer sheaths (Francis et al. 1978; Schieber et al. 2008), extracellular polymeric substances (EPS) (Francis et al. 1978; Orange et al. 2009), S-layers (Kish et al. 2016; Miot et al. 2017; Orange et al. 2009, 2011), peptidoglycan cell wall polymers (Westall 1997), on particulate organic matter (Oehler 1976) and as complete permineralization (Oehler and Schopf 1971).

The fossil evidence for the earliest life on earth might well be expected to include methanogenic archaea. Methanogens were the first archaea recognized as a group separate from other bacteria, and their metabolism was thought to be one of the first viable on the primordial Earth (Burggraf et al. 1991). Indeed, putative methanogens have been tentatively identified in ~3.42 Ga hydrothermal vent rocks from the Barberton Greenstone belt, South Africa (Cavalazzi et al. 2021) and there is isotopically light methane of presumed biogenic origin in ~3.5 Ga fluid inclusions from the Pilbara Craton, Australia (Ueno et al. 2006). This evidence, together with independent phylogenetic studies (Battistuzzi et al. 2004; Nitschke et al. 2013), suggests that methanogens existed on the Archaean Earth.

One of the key differences between archaea and bacteria is their cell wall structure (Figure 1). Archaea lack peptidoglycan, a major structural polymer in bacterial cell walls. Many archaea have an outer crystalline layer composed of proteins or glycoproteins with various 2-dimensional symmetries called an S-layer, which acts as a molecular "sieve" that cloaks the outside of the microbe (Schultze-Lam et al. 1996). The S-layer is not unique to Archaea but has been found in some bacterial genera, nor are S-layers ubiquitous within the archaeal domain. For example, the order Methanobacteriales lacks an S-layer and instead possesses a layer of pseudomurein, similar in structure to the murein that makes up the peptidoglycan in the bacterial cell wall (Meyer and Albers 2020). Both pseudomurein and peptidoglycan have a polysaccharide backbone linked by peptides, but the former is made up of N-acetylglucosamine (NAG) and N-acetyltalosaminuronic acid (TAL) whereas the latter is made of NAG and N-acetylmuramic acid (NAM). They also differ in the type of peptide links between sugars, where pseudomurein contains L-amino acids and peptidoglycan D-amino acids. It is these cell wall polymers found in peptidoglycan, pseudopeptidoglycan, and S-layers that offer the carboxyl, phosphoryl, and hydroxyl sites on which minerals can often nucleate (Ferris et al. 1988; Schultze-Lam et al. 1996; Frankel and Bazylinski 2003; Konhauser et al. 2004; Roberts et al. 2004; Benning et al. 2005; Orange et al. 2009). The differences in the chemical and physical structure of the cell walls may lead to varying degrees of mineralisation, potentially resulting in taphonomic biases (Francis et al. 1978; Peel 1988). For example, gram-positive bacteria have been argued to silicify more readily than gram-negative bacteria because of their thicker peptidoglycan layer, which results in a more negative surface charge (Westall 1997). Furthermore, both gram-positive bacteria and archaea with pseudopeptidoglycan cell walls have the sugar polymer as the outermost layer of their cell wall, making it available to surrounding aqueous chemical reactions. On the other hand, gram-negative bacteria have an outer membrane that constitutes an additional layer of protection against environmental stress and removes the peptidoglycan from direct contact with its surroundings. In fact, archaea with pseudomurein in place of murein also stain gram-positive (Boone 2015) which could imply that a pseudomurein wall also mineralises differently than S-layers. S-layers are also often the outermost layer, but since they are composed of proteins and not saccharides, they will likely interact with minerals in a different way.

Here we compared and contrasted the extent of mineralisation of carbonate, phosphate, and silicate on a strain of the filamentous methanogen *Methanobacterium* sp. (close resemblance *M. oryzae*). This strain is of interest for several reasons. Its morphology superficially resembles many filamentous

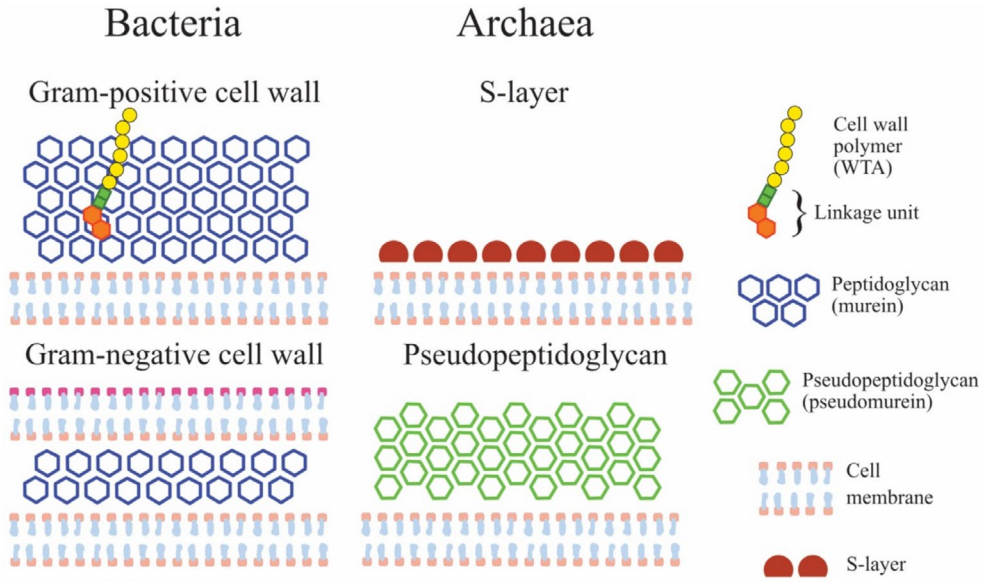

FIGURE 1 | Diagram of cell wall differences between bacteria and archaea. Modified with permission (Swoboda et al. 2010).

structures, both abiotic and biological, found in the rock record (e.g., McMahon 2019; Cavalazzi et al. 2021), as well as organic filamentous biomorphs formed in the lab (Cosmidis and Templeton 2016; Nims et al. 2021). In addition, it was isolated from a low-temperature serpentinizing environment (Neubeck et al. 2017) which may have been important to early life and analogous to conditions on several other planetary bodies (do Nascimento Vieira et al. 2020). Furthermore, this genus of archaea belongs to the order Methanobacteriales and has a pseudomurein wall (Meyer and Albers 2020). This study aims to analyse the mechanisms of mineralisation on these surfaces as opposed to S-layers that have been studied previously (Orange et al. 2009; Kish et al. 2016).

The mineralising ions, carbonate, phosphate, and silicate were chosen due to the abundance of these minerals in nature and their association with fossilised microbes throughout Earth's history. Additionally, the serpentinizing environment from which *Methanobacterium* sp. was isolated is rich in phosphates and carbonates. Phosphatization experiments of various organisms have been carried out previously (Briggs 2003; Kish et al. 2016; Miot et al. 2017) but to our knowledge, none have been carried out on methanogens. Many previous taphonomic experiments have used silica, including studies of the silicification of methanogens (Orange et al. 2009), although not those with a pseudomurein cell wall. The analysis of calcification, phosphatization, and silicification in tandem allows for a direct comparison of three mechanisms in preserving microbial morphology and gives insights into how these precipitate in association with a pseudomurein cell wall, comparable in structure to that of bacterial peptidoglycan.

2 | Materials and Methods

2.1 | Methanogen Strain and Growth Medium

The strain used in the present study belongs to the genus *Methanobacterium* sp. The cells are rod-shaped to filamentous, approximately 300 nm in diameter and between one and several tens of micrometres in length. They are non-motile, with an optimum growth temperature of 40°C (min-max: 15°C–45°C) and pH 7. The strain was isolated from natural samples that were previously collected from Chimaera Seeps in Turkey, which is a serpentine-hosted system (Neubeck et al. 2017).

A medium buffered by bicarbonate (4.0 g/L) and phosphate (0.4 g/L) was used following Zehnder et al. (1980); modified by Schnürer et al. (1994). Yeast extract solution (0.2 g/L) was added to enhance growth. 18 mL of medium was portioned out into 118 mL bottles and sealed with rubber stoppers and metal caps. The overhead gas was vacuum pumped, and the gas was exchanged with N_2/CO_2 3 times to remove oxygen. Sterilization by autoclaving the bottles was carried out at 121°C for 20 min. 1 mL of vitamin with trace element solution and 1 mL of reducing sulphide- and carbonate-based buffer were added to each bottle to a final growth medium volume of 20 mL. The bottles were inoculated with 1 mL of stock *Methanobacterium* sp. and left for approximately 2 months at 37°C without shaking to allow growth under an H_2/CO_2 (80:20) atmosphere (to a final pressure of 0.8–1 bar) which was replaced every 2 weeks.

During the first round of mineralisation, phosphate minerals precipitated in all experimental setups. To mitigate this problem, new cultures were grown in a phosphate-poor medium. Instead of a double-buffered medium with both carbonate and phosphate, only carbonate was used to keep the pH of the medium at 7.4 (Paula et al. 2019). The only phosphate added was K_2HPO_4 (Merck) at a concentration of 0.14 g/L as a phosphorus source for the methanogens. Analogous experiments were set up in this low-phosphate medium in which cells of *Methanobacterium* sp. were mineralised with the same procedure and concentrations of the mineralising agent as in normal medium experiments.

2.2 | Mineralisation Procedure

Mineralisation experiments were carried out in the 118 mL incubation bottles containing the culture medium and cells of *Methanobacterium* sp. so that a supply of nutrients was available throughout the process. Thus, the methanogens were not prematurely lysed but remained intact through the onset of mineralisation processes as they likely would under natural conditions (Orange et al. 2009). Mineralising agents were added by injecting 1–2 mL of solutions when the methanogen cultures had reached a white cloudy appearance indicating that cell growth had occurred (optical density was not measured). Each set of experiments ran for 2 weeks, 1 month, and 3 months and at the same conditions as for culturing: 37°C and without shaking. No additional nutrients, cells, or mineralising agents were added throughout the duration of the experiments.

The concentration of the mineralising agents was adjusted to best mimic natural conditions. For silica, a concentrated Na_2SiO_3 (reagent grade, Sigma-Aldrich) solution was diluted, and 1 mL was added to a final silica concentration of 0.5 g/L according to Orange et al. (2009). Calcium carbonate was produced by the reaction of two solutions added separately: 1 mL of $CaCl_2$ (≥ 95%; Fluka Analytical, Sigma-Aldrich) with a final concentration in the bottles of 3.3 g/L and 1 mL of $Na_2CO_3.H_2O$ (Emprove Essential, Merck) with a final concentration of 0.14 g/L to approximate concentrations that might occur at a hydrothermal vent setting (Ludwig et al. 2006). Phosphate was similarly prepared by the reaction of separate solutions to obtain a final concentration of $Ca_3(PO_4)_2$ of 0.025 g/L, just above the saturation level (0.02 g/L). To achieve this, 1 mL of 11 g/L Na_2HPO_4 (EMSURE) followed by 1 mL of 6.5 g/L $CaCl_2$ (≥ 95%; Fluka Analytical, Sigma-Aldrich), was added to the bottles.

In order to determine the saturation level of calcium carbonate and silica required in the medium to overcome the unwanted precipitation of phosphate, additional bottles of these two mineralising agents were prepared with a higher concentration (32.5 g/L and 2.14 g/L respectively) and left for 1 month. For the silica solution, the stock solution concentration remained the same (11.3 g/L), but 5 mL was added to reach a five-fold higher concentration of silica in the bottles.

Control samples containing only medium were mineralised in the same way as the experimental samples. Three additional controls with only methanogens and no mineralising agent were prepared. Two of these had normal medium, of which one was inoculated and left to grow for approximately 2 months to a

visible cloudy culture in the bottle and the other for 1 year, both without feeding. The third was a low-phosphate medium that was inoculated and grown for 2 months. Finally, one blank sample containing only medium was prepared. Figure 2 shows the experimental set-up described here.

2.3 | X-Ray Diffraction (XRD)

XRD analyses were carried out on 1-month samples of methanogens with carbonate, phosphate, and silicate experiments in normal medium. In addition, analyses were done on control samples without methanogens but with mineralising agents and on the two 1-month samples with increased concentrations of carbonate and silica. In the majority of samples, the precipitate obtained from experiments was only a few mg. This was thinly spread on glass micro-fibre filters, rinsed twice with distilled water, and left to air-dry overnight. A non-paper filter was used so as to avoid the presence of crystalline cellulose in the XRD patterns. To analyse, a sample holder with adjustable height was used in order to get the samples as flat as possible. The height was calibrated with a blank filter. A control XRD spectrum was taken on the blank filter to evaluate the input of an amorphous silica signal from the filter. In some cases, the precipitate was enough to scrape off and was ground in ethanol with a pestle and mortar and spread in a thin layer on a conventional powder sample holder, thus eliminating the background signal from the filter.

Analyses were carried out on a Bruker D8Powder diffractometer with Cu Kα radiation, Lynxeye XE-T PSD detector, with a working voltage and current setting of 40 kV and 45 mA. The range was between 20 and 80 with incremental steps of 0.2 2θ for an overall analysis time of approximately 20 min.

2.4 | Preparation for Scanning and Transmission Electron Microscopy (SEM and TEM)

Solid samples were collected at the end of each experimental duration by pouring out the contents of incubation bottles onto paper filters, vacuum suctioned, and rinsed with deionized water. Subsequently, the cells were prepared for SEM by fixation in a solution of 2.5% glutaraldehyde (25% solution; Sigma-Aldrich) and 0.1 M phosphate-buffered saline (PBS (Roche, Sigma-Aldrich); pH 7.3) for 4 h (Passey et al. 2007). The filters were washed of excess glutaraldehyde by submerging them three times for 10 min each in 0.01 M phosphate-buffered saline (PBS; VWR). Drying of the samples was carried out according to Araujo et al. (2003) by placing the filters in an ethanol series with increasing ethanol/distilled water concentrations of 50%, 70%, 80%, 90%, 95%, and 100%, allowing 10 min for each step and repeated 3 times in pure ethanol. A final dehydration step using HMDS (≥ 99%; Sigma-Aldrich) was done by submerging the filters once for 30–60 s followed by air-drying. Samples were thereafter coated with

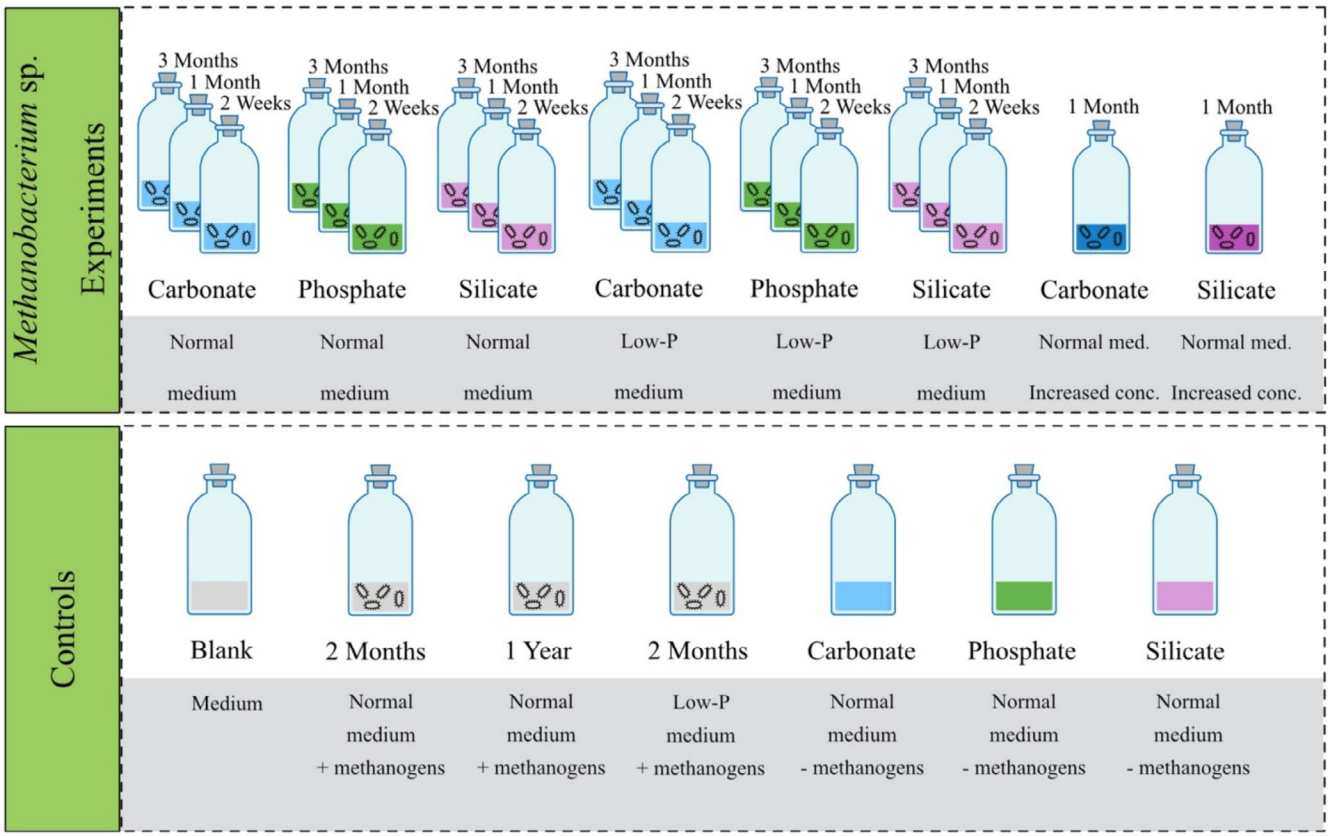

FIGURE 2 | Experimental set-up and controls. Low-P = low-phosphate. Normal medium was double buffered with both carbonate and phosphate. Low-P medium samples were buffered only with carbonate. Coloured bottles represent experiments with a mineralising solution (carbonate, phosphate, silicate). Bottles with increased concentration contained additional carbonate or silicate mineralising solution to overcome the precipitation of phosphates, which otherwise occurred in all experimental setups (excluding just medium).

a gold–palladium mix for analysis with a high-vacuum Zeiss Supra 35VP (Carl Zeiss SMT, Oberkochen, Germany) field emission SEM, equipped with an Ametek Apollo X EDX spectrometer located at Uppsala University. Beam settings for imaging were set at 4 kV and an aperture of 30.0 μm at an optimal working distance of 8.5 mm. For elemental analysis, these settings were changed to 20 kV and 60.0 μm.

Preparation for TEM began in the same way as for SEM, with a fixation and drying process using 2.5% glutaraldehyde and an ethanol drying series finished with HMDS. Small sections of the dried filters were cut out or, if enough material was present, they were picked off and embedded in epoxy resin using EpoThin 2 Resin and EpoThin 2 Hardener (Buehler). The resin blocks were trimmed, and ultrathin slices (50–70 nm) were cut to get a cross section of the filter using a Leica UC7 Ultramicrotome at the Rudbeck Laboratory, Uppsala. Slices were placed on grids and contrasted in 5% uranyl acetate and Reynold's lead citrate for 10 and 2 min respectively. Dried grids were examined in a Tecnai G2 Spirit BioTwin transmission electron microscope (Thermo Fisher/FEI) at 80 kV with an ORIUS SC200 CCD camera and Gatan Digital Micrograph software.

3 | Results

Precipitation of minerals began in all 3 experimental setups already at 2 weeks and became increasingly abundant at the 1- and 3-month stages (Figures 3–7). Additionally, phosphatic precipitates were identified in all experiments, including controls (Figures 3, 7), in the form of granular sheets and spheres. Their composition was evident by the overwhelming presence of Ca, P, O, and C in EDX spectra and the unambiguous identification of hydroxyapatite in XRD patterns (Figure 3b; Figure S1). Carbonate and silicate mineralising experiments also contained calcium carbonate crystals (Figures 3a, 4f) and silica precipitates, respectively (Figures 3c, 6c,f). The growth in the two different types of medium, normal and low-phosphate, was monitored by methane measurements over a 2-month period, and no significant differences in growth rate were observed, meaning that methanogens grew equally well in both (Figure S2).

In many samples, it was possible to observe very long and thin filaments around the methanogens that were minute in diameter (~80–100 nm) but several tens of micrometres long (Figures 4d,e, 5f). These were particularly common where methanogens were grown in low-phosphate medium with added phosphate mineralising agent (Figure 5f). They had a uniform diameter but were sometimes a little flattened, especially when embedded in minerals.

Table 1 contains a summary of the morphological and chemical characteristics of the products of the mineralisation experiments.

3.1 | X-Ray Diffraction

XRD patterns in the carbonate samples reveal the presence of calcite (Figure 3a). The very characteristic peak for the d-spacing 3.03 Å of the (104) lattice plane is present (Kontoyannis and Vagenas 2000). Additionally, d-spacings 3.85 Å, 2.49 Å, 2.28 Å, 2.09 Å, 1.91 Å, and 1.87 Å that represent the (102), (110), (113), (202), (108), and (116) lattice planes respectively are also present (Gunasekaran et al. 2006). The peaks that correspond to a diffraction angle 2θ of around 26° and 32° in the C1M are related to the lattice planes (002) and (211) with d-spacings 3.42 Å and 2.77 Å respectively in hydroxyapatite (Curran et al. 2011). These peaks are also present in the phosphate samples.

The XRD patterns of the phosphate samples at 1 month are shown in Figure 3b. Many of the peaks coincide with known peaks for hydroxyapatite, like the (002) and (211) lattice planes (Bigi et al. 2007; Curran et al. 2011). The broadness of the peaks in the diffractograms of the phosphate samples relative to the standard spectrum taken from the RRUFF database is due to a lower crystallinity. The XRD pattern for the abiotic phosphate control sample (P1M control), i.e., no methanogens but added phosphate mineralising agent, is comparably more amorphous than the others, with less defined peaks (Figure 3b).

The silica samples show a similar trend to one another with a hump at the beginning of the diffractograms (Figure 3c). In the majority of cases, the precipitate obtained from experiments was only a few milligrams and thinly spread on a filter. The filters used to collect precipitate for XRD were glass microfibre, and a control XRD pattern was taken on a blank filter, which showed a similar initial hump in the diffractogram to the ones seen in the silica samples. The increased silica concentration sample (Si1M+++) had enough precipitate that it was possible to scrape it off and analyze on a normal powder sample holder. Thus, the filter paper signal was eliminated. Nonetheless, the diffraction pattern for this sample shows an intense, albeit broad, peak at around 23°2θ that, to some extent, overlaps the filter signal (seen in Si1M and Si1M control). These signals at the beginning of the pattern indicate silica in a relatively poorly crystalline phase (Brichni et al. 2016; Maryani et al. 2018).

3.2 | Calcium Carbonate Mineralisation Experiments

Most filaments at 2 weeks remained uncoated and were intact and turgid (Figure 4a,b). Precipitation of calcium phosphate occurred in the form of micro-metre crinkly spheres that were between 1 and 4 μm in diameter (Figure 4a,b). From these, precipitates began to wrap around the filaments (bottom arrow in Figure 4a). The few filaments completely coated in this way were irregular in shape (top arrow in Figure 4a) and larger in diameter with respect to the original filament (from 240 nm in naked filaments to 420 nm when coated). A few large, elongated crystals 160 μm long and 35 μm wide were observed. 1-month samples showed larger sheets of a granular precipitate identified as calcium phosphate in EDX with a small amount of Na. In this precipitate, elongated crystals were present identical to those found in 2-week samples but smaller (40 μm long and 10 μm wide) (Figure 4c). These had EDX spectra consistent with calcium carbonate, and XRD confirmed the presence of calcite (Figure 3a; Figure S1). Methanogens were present here, somewhat embedded, but not abundant and were only found in the phosphatic precipitate, not the calcite crystals. The carbonate sample after 3 months showed extensive granular precipitate with only the occasional methanogen present, and these were usually very degraded.

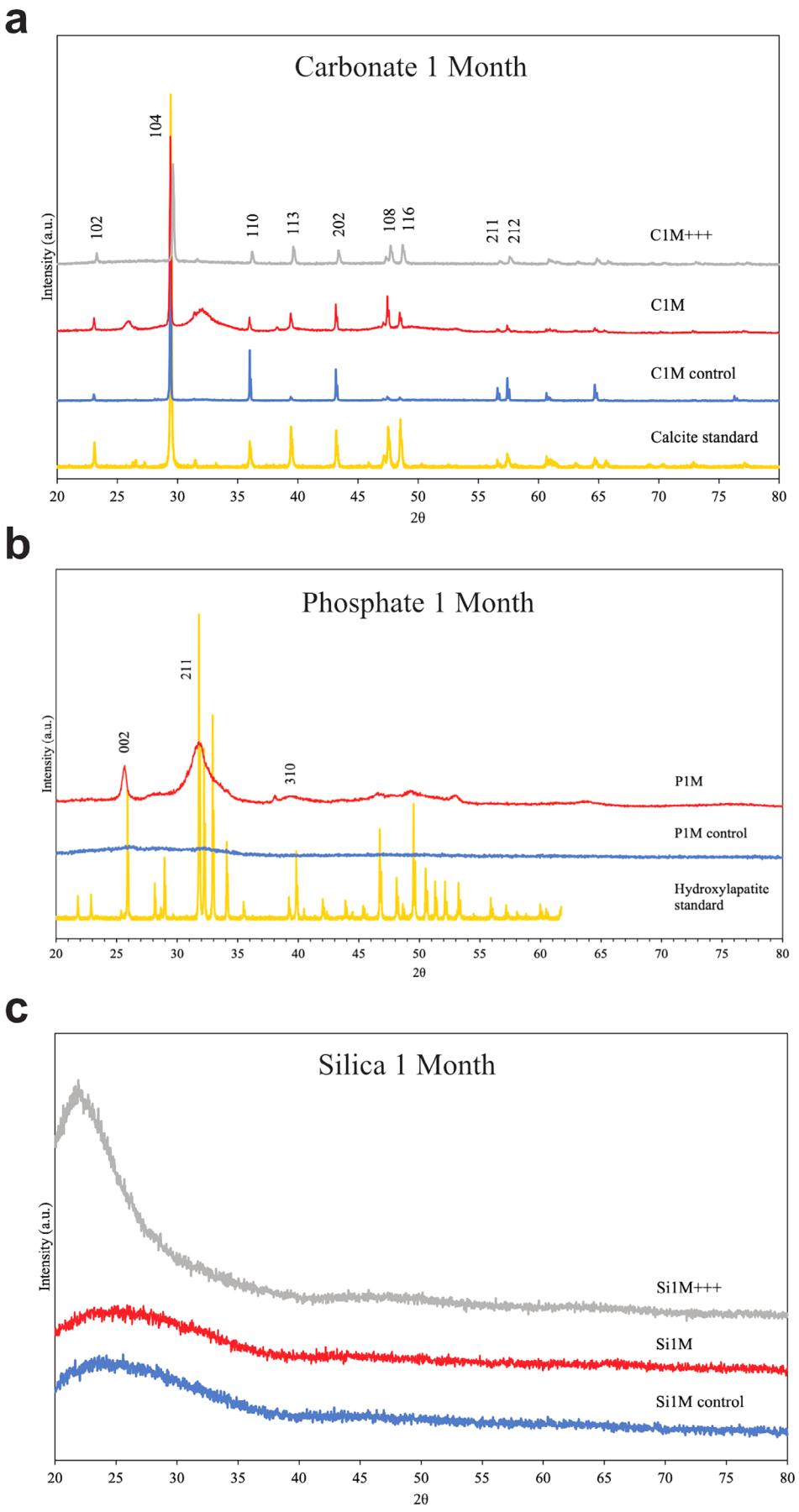

FIGURE 3 | XRD patterns of experiments at 1 month (1M), controls without methanogens at 1 month (1M control) and increased concentration experiments (1M+++) for (a) carbonate, (b) phosphate, and (c) silica.

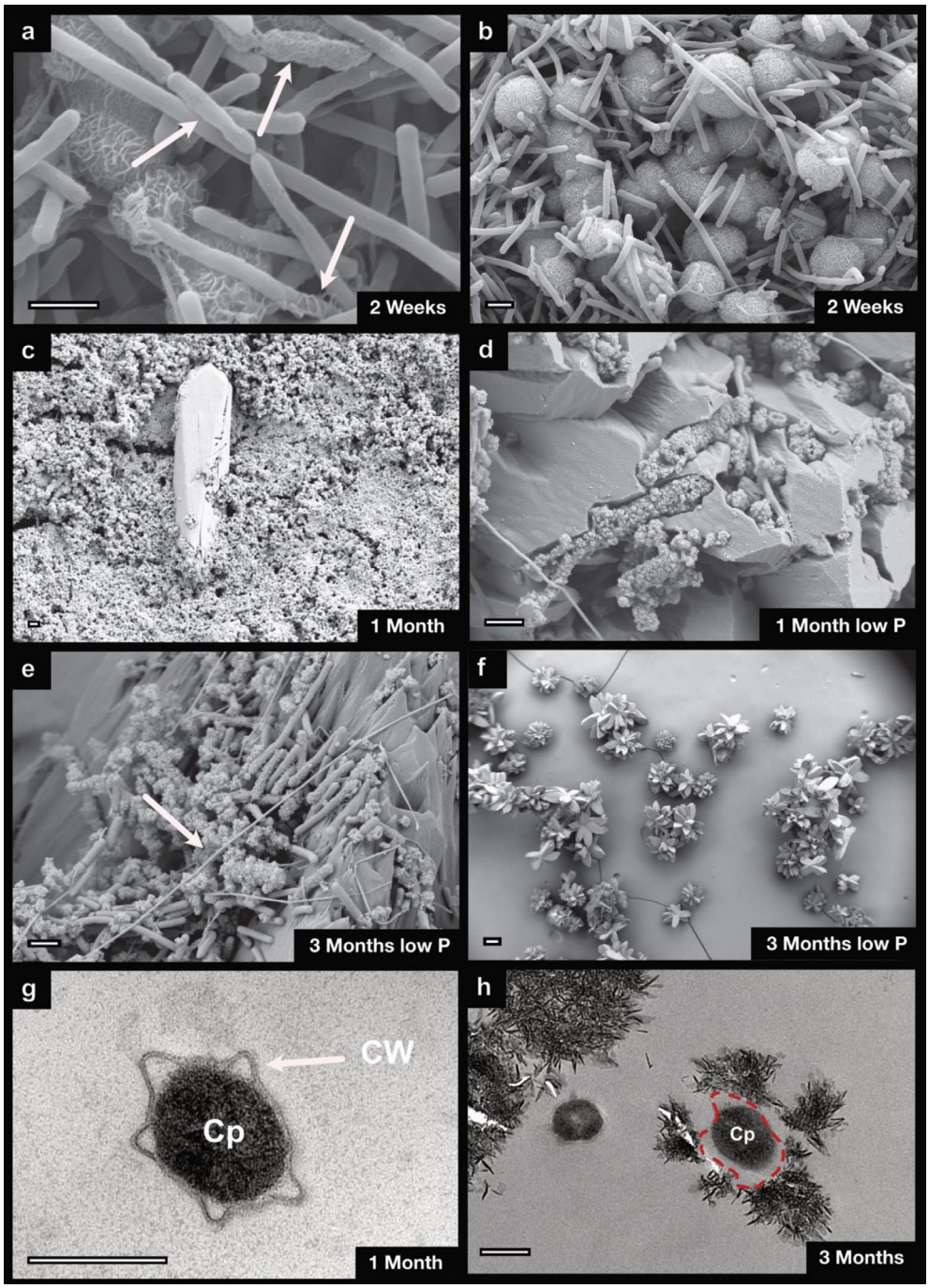

FIGURE 4 | (a–f) SEM images of *Methanobacterium* sp. mineralised in carbonate solution at various time intervals. (a) Arrows in the image indicate a coated filament (top), a degraded filament (middle), and one in the process of being coated (bottom). (b) Overview of filaments and rods growing on top of spherical precipitates. Most are uncoated and turgid. (c) Calcite crystal. (d) Coated filament embedded in calcite crystal in low-phosphate medium. (e) Coated and uncoated filaments in low-phosphate experiment. Arrow indicates long minute filament. (f) Calcite crystal aggregates. (g, h) TEM images of experiments in normal medium. Cp, cytoplasm; CW, cell wall. Dotted red line in (g) highlights the CW. Scale bar SEM = 1 μm (with the exception of f = 100 μm); TEM = 200 nm.

In low-phosphate bottles, and at all time intervals, large star-shaped mineral clusters made of the same elongated calcium carbonate crystals as mentioned previously (up to ~350 μm cluster size) were seen (Figure 4f). These crystals were more abundant than in normal medium samples and often had clumps of granular phosphatic precipitate on them where trapped methanogens could be found. Methanogens were more often coated in this granular precipitate than in other carbonate samples. The coating had the same rough granular exterior (Figure 4d,e) and a significantly larger diameter than uncoated cells (from 300 to 700 nm). Occasionally, coated methanogens could be seen trapped in a larger calcite crystal (Figure 4d). Methanogens were still visible, some coated and some naked at the 3-month stage (Figure 4e).

TEM images of mineralised methanogens at the 1- and 3-month stage showed a precipitate on and around the microbes with a

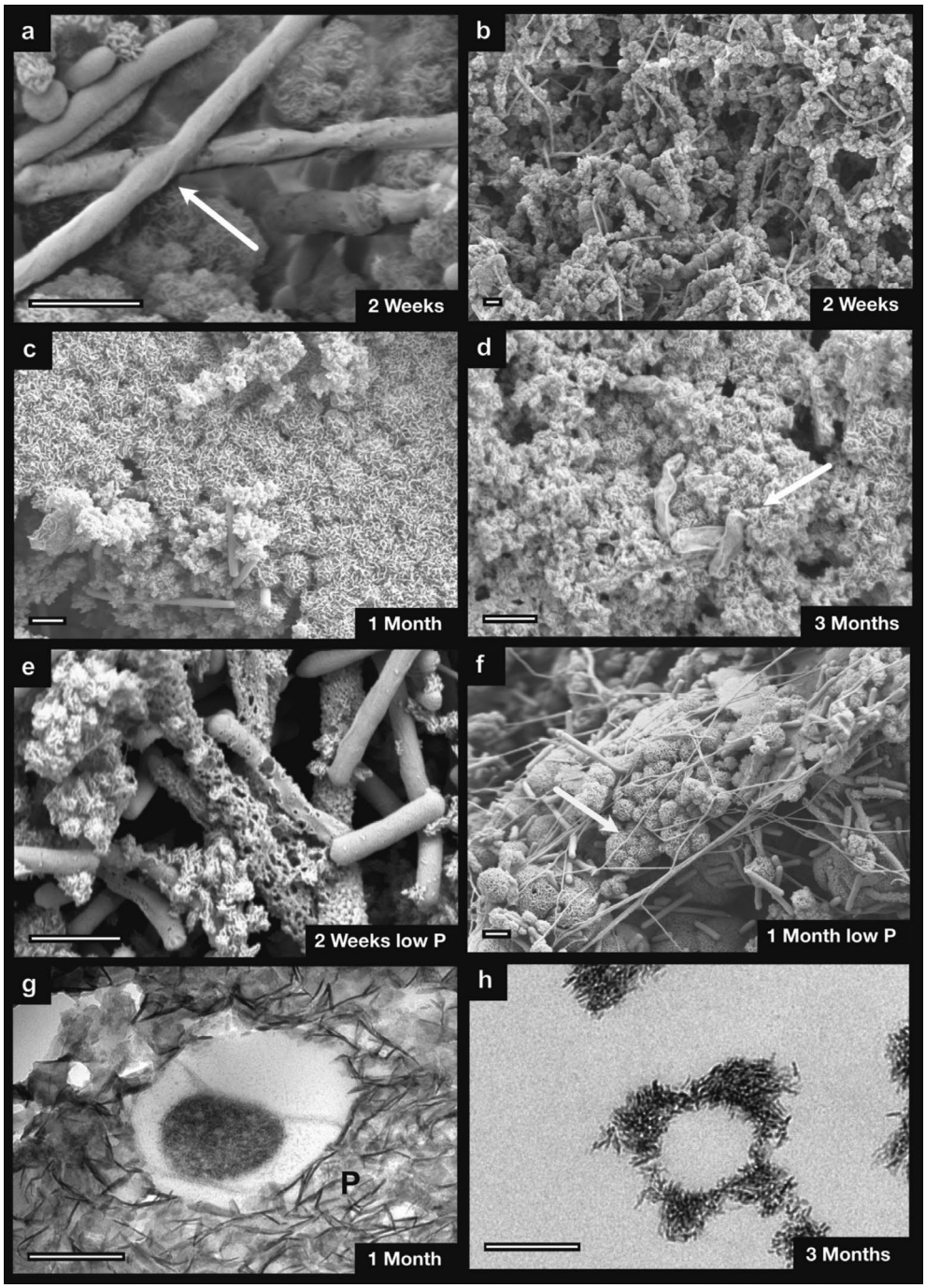

FIGURE 5 | (a–f) SEM images of *Methanobacterium* sp. in phosphates at various time intervals. (a) Filaments starting to degrade (arrow). (b) Some filaments still turgid and others with thick globular coatings. (c) Sheets of granular precipitates at 1 month with few methanogens. (d) Degraded methanogens at 3 months (arrow). (e) 2-week samples in low-phosphate medium. Note the coated filament in the back (right). (f) Lots of turgid cells visible in 1-month low-phosphate medium. Note the much thinner filaments (arrow). (g, h) TEM images in normal medium. P, phosphate. Scale bar SEM = 1 μm; TEM = 200 nm.

plate-like structure (Figure 4h). No preferred orientation of the plates could be seen in association with the cell walls (i.e., parallel or perpendicular with respect to the cell wall). Precipitates formed both in association with the cells and separately (Figure 4h). However, they did not penetrate inside the cell walls (Kish et al. 2016), nor did the precipitates proceed inside the cells. As precipitates swamped the cells, not just the cytoplasm detached from the cell walls (Figure 4g), but the cell walls also detached from the precipitate (Figure 4h).

3.3 | Phosphate Mineralisation Experiments

At 2 weeks, many filaments were still uncoated but had some small wrinkles on the surface (arrow in Figure 5a). Figure 5b shows an overview with many filaments completely covered in a very globular and irregular phosphatic precipitate (Figure 3b). At the 1-month stage, the precipitates formed larger sheets (Figure 5c) with some methanogens still visible. The cells were largely uncoated with a smooth and turgid

TABLE 1 | Summary of morphological and chemical traits of mineralised methanogens at different time intervals in normal double buffered medium and low-phosphate medium.

Mineralising solution	Time	Normal medium	Low-phosphate medium	Composition of minerals (EDX/XRD)	Figure number
Calcium carbonate	2 weeks	Cells turgid. Wrinkly spheres of precipitate 1-4 μm in diameter with some wrapping around the cells	Star-like mineral clusters of elongated crystals. These occasionally had clumps of a granular precipitate on them	Granular/spheres: Ca, P, O, C, Na; hydroxyapatite; Crystals: Ca, C, O; calcite	Figure 4a,b
	1 month	Some cells still visible but not abundant. Large sheets of granular precipitate; some elongated crystals	Methanogens sometimes coated in the precipitate. Similar results for all three time-periods	Sheets: Ca, P, O, C, Na; hydroxyapatite; Crystals: Ca, C, O; calcite	Figures 4c,d,g and 3a; Figure S1
	3 months	Few methanogens left, still turgid but small. Embedded in sheets of precipitate	Methanogens still present, some coated some naked	Ca, P, O, C, Na; hydroxyapatite	Figure 4e,f,h
Calcium phosphate	2 weeks	Many filaments uncoated, some with surface wrinkles. Many engulfed in precipitate. Either wrinkly spheres or globular/rough precipitates on the methanogens	Both whole and degraded filaments present, some coated in granular precipitate. Spherical precipitates present	Ca, P, O, C, Na; hydroxyapatite	Figure 5a,b,e
	1 month	Methanogens less visible. Globular sheets and extensive granular precipitates	Many spherical precipitates clumped together on which methanogens could be found. Many still whole and turgid. Several long and very thin filaments (< 100 nm in diameter) present around the methanogens	Ca, P, O, C, Na; hydroxyapatite	Figures 5c,f,g and 3b; Figure S1
	3 months	Very few small and deflated methanogens visible. Large sheets of precipitates swamp the methanogens	Large sheets of granular precipitate, also partly made of spheres, with relatively abundant methanogens	Ca, P, O, C, Na; hydroxyapatite	Figure 5d,h
Silica	2 weeks	Many filaments coated in uniform sheath increasing overall diameter. Naked filaments still turgid. 2 types of precipitate: one more smooth but grainy coating, and one more clumpy	Grainy but relatively uniform coatings on the filaments. Many filaments still uncoated and turgid	Smooth: Si, O, C; amorphous silica; Clumpy: Ca, P, O, C; NA	Figure 6a,d
	1 month	Filaments snugly coated in smooth precipitate, still not showing particular signs of degradation. 2 types of precipitate: sheets of smoother precipitate and wrinkly spheres glued together	Similar to 2 weeks. Methanogens either uniformly coated or embedded in smooth silica precipitate. Some filaments with surface wrinkles	Smooth: Si, O, C; amorphous silica; Spheres: Ca, P, O, C, Si, Na; NA	Figures 6b,c and 3c; Figure S1
	3 months	Fewer filaments present, a few on top of and coated in precipitates that are still turgid. Large sheets of precipitate that coat everything, spheres present and mostly coated in wrinkles	Abundant filaments still present, of which many are uncoated and turgid. Similar coatings as earlier stages but much thicker in diameter (up to 1.4 μm)	Smooth: Si, O; amorphous silica; Spheres: Ca, P, O, C, Na; NA	Figure 6e,f

exterior, although swamped in precipitate. At 3 months, this precipitate extended further, and methanogens were fewer and very degraded (arrow in Figure 5d). For all types of precipitate, EDX spot analysis revealed mostly Ca, P, O, and C (Figure S1). Overall, precipitation onto filaments was somewhat globular and rough or precipitated as sheets or spheres with methanogens on top (Figure 5b–f).

In parallel, in the low-phosphate medium samples where a phosphate mineralising agent was added, the same spherical precipitates appeared as in previous samples grown in normal medium, but these rarely coated the methanogens. Several cells remained intact and turgid while some began to lyse (Figure 5e). Abundant small string-like filaments were visible, about one third of the diameter of the methanogens (80–100 nm as opposed to ~300 nm) (Figure 5f). At 3 months, many cells were still scattered around on and embedded in the precipitate. However, they did not generally have a uniform coating.

In TEM images, the cells were surrounded by the same platelike precipitate seen in carbonate samples (Figures 4h and 5g,h). Similarly, cell walls detached from the precipitate (Figure 5g) and at 3 months, empty moulds could be seen (Figure 5h).

3.4 | Silica Mineralisation Experiments

In the silica mineralisation experiments, many cells at the 2-week stage were already coated in a very uniform and smooth precipitate relative to carbonate and phosphate experiments (Figure 6a). There were also two different types of mineral precipitation. The first type encrusted the filament completely and created a uniform coating with a slightly grainy texture. This coating significantly enlarged the diameter of the filament (from ~0.25 μm to 0.7 μm) (top arrow in Figure 6a). The second type of precipitation created globules of non-uniform crystals that swamped the filaments and created a much rougher and irregular outer surface (bottom arrow in Figure 6a). EDX spot analysis has a resolution of 1 μm so it cannot resolve these coatings (< 0.5 μm). In the 1-month silica samples, there was a clear distinction between the two types of precipitate. Large crinkly spheres very similar to those found in the carbonate and phosphate experiments precipitated around the methanogens (Figures 4b, 5f, 6b). EDX spectra of these showed large amounts of Ca, P, O, and C with less Si (Figure S1). The smooth precipitate seen in the 2-week samples was more extensive here and formed sheets (Figure 6b,c). According to EDX analysis, the latter was almost exclusively composed of Si, O, and C (Figure S1) and XRD spectra confirmed the presence of amorphous silica (Figure 3c). The spherical precipitates had methanogens lying on top of them, rather than embedded (Figure 6b), whereas the smooth sheets of silica coated the filaments more snugly, reproducing their overall morphology (Figure 6c). At 3 months, some filaments were still visible. The substrate in which the filaments were embedded was made of the rougher phosphatic sheets and a few wrinkled spheres.

Low-phosphate samples also had many filaments that were covered in relatively uniform precipitate coatings starting already at 2 weeks (Figure 6d). As time progressed, the coatings thickened to as much as 0.8 μm and even 1.4 μm in one case (Figure 6e). Low-phosphate medium samples also contained spherical precipitates, although they were somewhat less abundant than in the normal medium.

Silica samples in TEM showed a fluffy precipitate on and around the cells (Figure 6f). In these, the cytoplasm was not detached from the cell wall even at the 3-month stage. The precipitate

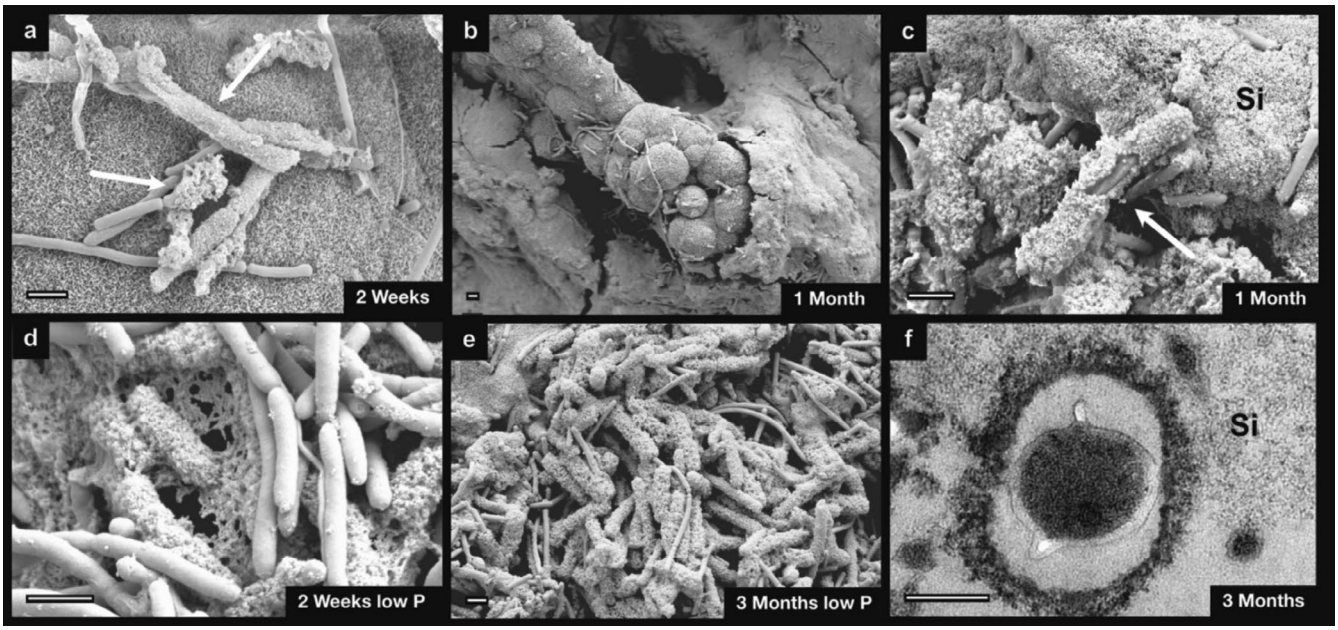

FIGURE 6 | (a–e) SEM images of *Methanobacterium* sp. mineralised in silicate at different time intervals. (a) Some coated (arrows) and uncoated filaments. A relatively smoothly coated filament has more than doubled in diameter (top arrow). (b) Detail of phosphate spheres in smooth silica precipitate. (c) Close-up of almost completely coated filament. Note the large size compared to nearby filaments. (d, e) Methanogens in low-phosphate samples that were relatively uniformly coated. At 3 months (e) the coatings were much thicker. (f) TEM image of methanogen at 3 months. Note the ring of denser precipitate around the cells. Si, silica. Scale bar SEM = 1 μm; TEM = 200 nm.

often did not form directly in contact with the cell wall but a few nanometres from the surface, creating a halo. The silica was widespread and did not precipitate only on isolated methanogens, but where cells were present and embedded, a ring of more dense precipitate formed relative to the surrounding silica (Figure 6f).

Additional experiments were made for samples in carbonate and silicate in which the concentration of these two mineralising solutions was increased in order to overcome the precipitation of phosphate from the medium. Samples with increased carbonate solution mostly precipitated calcite crystals, and few methanogens were visible (data not shown). For the increased silica samples, the same two types of precipitate were observed as in previous silica experiments, and several filaments were coated. However, a key difference was the presence of holes in the phosphatic spherical precipitates that were identical in size and shape to the methanogens themselves (Figure 7a,b). A small piece of a cell wall was visible stuck in one of these moulds (Figure 7a).

3.5 | Controls

Abiotic control samples consisted of 3 bottles without methanogens but with added mineralising agents. Two additional controls containing only methanogens and no mineralising agent were prepared and kept for 2 months and 1 year (Figures 2, 7) in normal medium. Finally, one control with only methanogens was kept in low-phosphate medium for 2 months. In abiotic controls with added carbonate mineralising agent, calcium carbonate crystals could be found (Figure 3a). These crystals were more abundant than in carbonate samples containing methanogens. The phosphate control was covered in large sheets of calcium phosphate which displayed desiccation cracks (Figure 3b). Finally, the silica control sample had a small grain identified as silica in EDX and XRD and in this case phosphate was less abundant, to be found only stuck in the fibers of the filters rather than large sheets (Figure 3c).

In controls with methanogens but no added mineralising agent, granular and spherical precipitates formed that had very similar morphologies to those in the mineralising experiments (compare for example Figure 7d with Figure 4b or Figure 7d,e with Figure 5b,f). The 2-month samples contained more turgid and intact cells but nonetheless had precipitates on them (Figure 7c). In contrast, methanogens in the 1-year-old sample had more wrinkly surfaces indicating the beginnings of lysis or death, and some were visibly degrading (arrow in Figure 7f). Precipitates were much more widespread than in the younger sample. Despite this, methanogens were still present. Phosphate precipitates also formed in the low-phosphate control (Figure S3).

4 | Discussion

The purpose of these experiments was to analyze how three common minerals found on Earth's surface would precipitate and interact in association with a methanogen of the genus *Methanobacterium*. *Methanobacterium* is especially interesting because it lacks an S-layer and instead has pseudomurein, a compound similar to bacterial peptidoglycan (Meyer and Albers 2020).

The pH of all experiments was well buffered and unlikely to change through time, despite the addition of external mineralising agents. Previous work has attempted to define the pH tolerance of this species of methanogen, without success, since the buffer is so strong (Stephens 2023).

In all experiments, mineral precipitation onto cell walls began immediately on some filaments while others remained uncoated

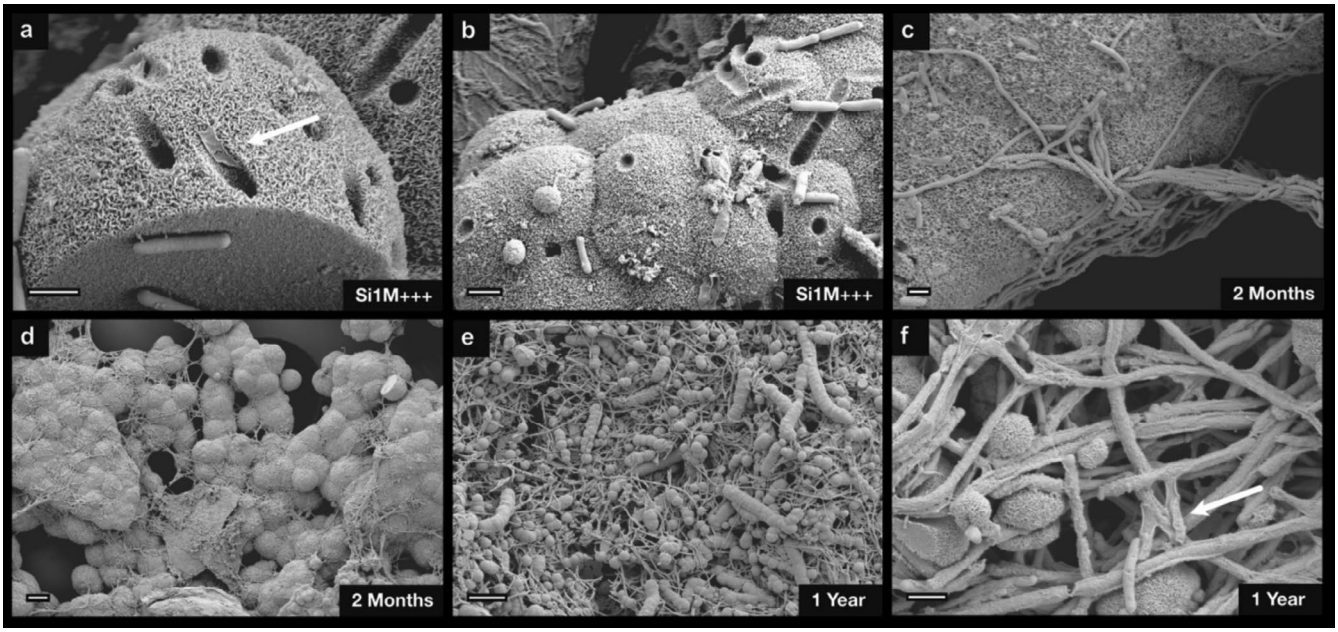

FIGURE 7 | SEM images of controls. (a, b) Samples with increased silica concentration. Note the moulds left in phosphate precipitates by methanogens. Arrow in (a) indicates a piece of cell wall. (c–f) Methanogens grown for 2 months (c, d) and 1 year (e, f) without mineralising agent. Arrow in (f) indicates a degraded filament. Scale bar (a–c, f) = 1 μm; (d, e) 10 μm.

well into the third month. This has been noted before (Lalonde et al. 2005; Orange et al. 2009; Kish et al. 2016; Gaboyer et al. 2017) and it has been suggested that uncoated cells are still viable but perhaps in a dormant state in which mineralisation is suppressed (Orange et al. 2009). Dormancy may have been induced by nutrient starvation since neither headspace gases nor other nutrients were replenished after the first day of mineralisation. In the majority of samples, many filaments remained intact and turgid, further suggesting that they were still viable. Several had wrinkles on their surface indicating the beginnings of lysis (Figure 5a) and the detachment of the cytoplasm from the cell wall could be seen in TEM (Figures 4g, 5g). A study by Katsen-Globa et al. (2016) on the methods of HMDS drying showed that around 3 min in HMDS does not cause any structural change in the cells. The cells here were only kept for 30–60 s, so artefacts of the TEM drying process do not account for the observed deformation.

The minute filaments seen in several samples (Figures 4e, 5f) are notably longer and thinner than the methanogens. These structures are most likely fimbriae. Fimbriae have several different possible functions, among them the formation of biofilms. Similarly to cyanobacteria, biofilm production may be a stress response to adverse conditions such as starvation or the presence of minerals in solution (Cassier-Chauvat and Chauvat 2014). However, these structures were very abundant in the low phosphate samples with added phosphate mineralising agent where cells were likely less stressed than in other samples. Fimbriae have also been observed in other archaea (Thoma et al. 2008) where they produce large fimbrial networks used to adhere to solid surfaces. Additionally, they have been noted in the *Methanobacterium* genus (Boone 2015).

4.1 | Mineralisation Mechanism and Morphology: Carbonate and Phosphate

The introduction of a calcium chloride solution into the medium reacted with bicarbonate and phosphate already present in the form of buffering agents in the following way:

$$2NaHCO_3 + CaCl_2 \leftrightarrow CaCO_3 \downarrow + 2NaCl + CO_2 + H_2O \quad (1)$$

$$2KH_2PO_4 + 3CaCl_2 \leftrightarrow 2KCl + Ca_3(PO_4)_2 \downarrow + 4HCl \quad (2)$$

$$Na_2HPO_4 + CaCl_2 \leftrightarrow 2NaCl + CaHPO_4 \downarrow \quad (3)$$

The reaction that occurred due to the addition of the phosphate mineralising agent was the same as Equation (2) above, whereas the one from the carbonate mineralising agent was as follows:

$$Na_2CO_3 + CaCl_2 \leftrightarrow CaCO_3 + 2NaCl \quad (4)$$

Considering the high concentration of Ca^{2+} added (3.3 g/L) coupled with the concentration of the bicarbonate (2.9 g/L) and phosphate ions (0.56 g/L) from the buffers, the resulting solution is supersaturated. This was evidenced by the fact that the medium turned cloudy immediately when calcium chloride was added. The EDX spot analysis of morphologically alike granular sheet-like precipitates in all the phosphate and carbonate samples showed the presence of Ca, P, O, and C, as well as minor amounts of Na (Figure S1). The broad peaks in the XRD pattern show a poorly crystalline calcium phosphate precipitate (Figure 3b) which is likely a precursor to apatite (Krajewski et al. 1994). Poorly crystalline globular precipitates have also been observed in precipitation experiments of phosphate associated with bacteria (Lucas and Prevot 1985) but never with methanogens. The EDX results from the large, elongated crystals in carbonate experiments (Figure 4c) indicate C, Ca, and O, and the XRD results show a calcite lattice produced by these crystals (Figure 3a; Figure S1). As previously mentioned, the (002) and (211) crystal lattice planes of hydroxyapatite are also visible. The less crystalline nature of the precipitate giving rise to these peaks is evidenced by the lower intensity when compared to the well-defined peaks of the calcite diffractogram due to a more random scattering of X-rays by materials lacking ordered crystal lattices.

The mechanism of calcite versus apatite precipitation has been referred to as a "switch" with local pH changes driving one precipitation over the other (Briggs 2003). Methanogens are known to induce calcium carbonate precipitation due to the removal of CO_2 in their metabolic process, thus locally increasing the pH (Roberts et al. 2004; Visscher and Stolz 2005). However, since calcite also precipitated in control samples without methanogens, it is difficult to determine the effect that methanogenic CO_2 fixation may have had on the precipitation of calcite. Comparing the XRD patterns of the abiotic controls with those of the 1-month samples containing methanogens (C1Mcontrol/P1M control and C1M/P1M, Figure 3a,b), the phosphate signals (002) and (211) are more clearly defined in samples containing methanogens. This suggests that the presence of methanogens had an effect on the crystallinity of the phosphate precipitate, whereas in their absence, the supersaturation alone caused the precipitation of amorphous calcium phosphate. Based on the solubility constants of calcium phosphate and calcium carbonate, it is likely that the latter, being less soluble, would precipitate first (Aylward and Findlay 1974). In several experiments, calcite crystals are overlain by phosphate precipitates (Figure 4c). On the other hand, the presence of biology can interfere with the normal chemical equilibrium, and phosphates may precipitate first due to the presence of nucleation sites on cell walls (Figure 4d).

Notably, methanogens grown in low-phosphate medium with added carbonate as a mineralising agent still had phosphate precipitates around them (Figure 4d,e). This could be because small amounts of phosphate inhibit the precipitation of calcite (Langerak et al. 1999), but calcite crystals were also present in these samples. The calcium from the added mineralising agent could have reacted with phosphate in the medium despite the low concentration. However, both normal medium and low-phosphate experiments with only methanogens and no mineralising agent also showed extensive precipitation of phosphates (Figure 7c–f; Figure S3). Precipitation began already in the control grown for just 2 months but was much more widespread in the sample grown for 1 year. In both, the phosphatic precipitates formed the classical spheres and also coated the methanogens (Figure 7d–f). Blank samples with only medium produced no precipitates. Once again, this points towards a methanogen-driven mechanism for the precipitation of phosphates. Methanogen-induced phosphate precipitation has, to our knowledge, never been documented.

Studies have indicated that the precipitation of phosphates can be controlled by prokaryotic cells and is not always merely passive (Benzerara et al. 2004). This latter conclusion is partly drawn on the orientation of apatite crystals and their close association within the cell wall and on the interior of bacteria, a phenomenon that was not observed here. The close-fitting coating of phosphates on and around the methanogens in many samples (Figures 4a,d,e, 5e, 7e) suggests a surface nucleation mechanism. In the case of bacteria, precipitation onto the cell wall is thought to be related to the presence of charged functional groups such as carboxyl, phosphoryl, and hydroxyl found in the murein (Beveridge and Murray 1980; Ferris et al. 1988). Additionally, the negative surface charge of bacterial and archaeal cell walls can attract cations such as calcium in solution that act as a bridge for the negatively charged phosphate anions, thus facilitating precipitation.

Peptidoglycan in bacterial cell walls is known to bind covalently via phosphodiester linkages to wall teichoic acids (WTA) (Swoboda et al. 2010). These cell wall polymers are found in gram-positive bacteria, and their function, though not completely understood, is vital to the survival of bacteria (Esko et al. 2009; Swoboda et al. 2010). The bonding site of the phosphodiester linkage is the C-6 hydroxyl of the N-acetyl muramic acid sugars. Similarly, the same hydroxyl site on the N-acetyltalosaminuronic acid of pseudopeptidoglycan could provide a binding site for phosphates (Figure 8). Consequently, the pseudopeptidoglycan cell wall of archaea may well be primed to bind to phosphate groups, which explains why phosphates precipitated on and around the methanogens in all samples, including those grown in low-phosphate medium and controls with only methanogens and no mineralising agent added.

This hypothesis predicts that precipitation would not occur on fimbriae, which have no surface charge or cell wall structure. Our observations satisfy this prediction. Only once was it possible to see a fimbria coated in precipitate, but this sample was embedded in the calcite grain and not coated in the granular phosphatic precipitate often seen coating the methanogen cells.

The possibility for acidophile and hyperthermophile archaea to passively induce precipitation of phosphates has previously been documented (Kish et al. 2016; Miot et al. 2017). Kish et al. (2016) outline a stepwise mechanism of the nucleation and precipitation of Fe-phosphates, similar to what is observed here. The initial stage is nucleation onto the cell surface, forming small patches of precipitate (Figure 4h) that multiply and, binding together, form a coating all the way around the methanogen (Figure 5h). The archaea that Kish et al. (2016) worked with have an S-layer, and it was possible to observe the hexagonal surface layer of this structure. In the present study, the interaction is presumably with the pseudomurein. Keighley et al. (2018) proposed a comparable mechanism for the formation of phosphatized globules in Eocene oil-shales. Following the death or lysis of cells and the release of P into waters, an apatite precursor may precipitate in the vicinity of the cell wall. Diagenetic alteration will transform the precursor into an apatite mineral and leave either a hollow pseudomorph of the cell wall or a mould of its interior. Of these two scenarios, the hollow void was observed here (Figure 5h) whereas later infilling of the void was not, though this may be just a question of time.

Another possible mechanism for the precipitation of phosphates is through passive precipitation in association with metabolites. The methanogens may secrete a variety of products that can react with compounds and induce precipitation of minerals (Frankel and Bazylinski 2003). This requires further investigation. A review by Krajewski et al. (1994) concludes that cells do not constitute a preferential substrate for the precipitation of apatite but that microbes do influence the concentration of reactive phosphate in sediments.

The precipitates coating the methanogens in carbonate and phosphate samples were very irregular, or globular, and did not outwardly reflect the morphology of the encapsulated microbe (Figures 4a and 5b). Interestingly, in experiments carried out in low-phosphate buffer medium with added carbonate, the methanogens were sometimes quite uniformly coated in phosphatic precipitate, as seen in Figure 4d,e, though the coating was very rough in texture. Some filaments were initially coated in this granular precipitate and *then* embedded in the larger calcite crystal that formed around them (Figure 4d). The precipitation of apatite followed by the overgrowth of calcite crystals has been previously documented (Briggs 2003). Fossil microbes in calcite may also be coated in different minerals, such as iron oxides, before being encapsulated in calcite (see possible examples in Trewin and Knoll 1999).

4.2 | Mineralisation Mechanism and Morphology: Silicate

Small grains of silica precipitate could be seen on the surface of the methanogens already at 2 weeks, which could be the

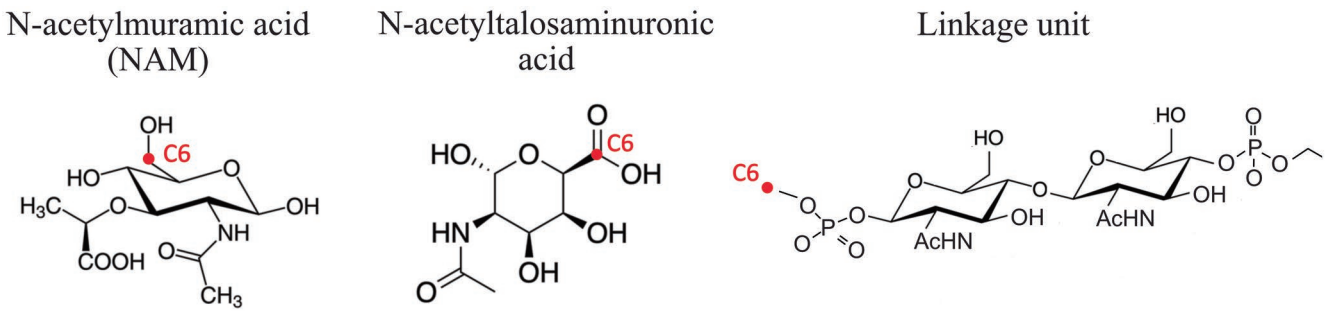

FIGURE 8 | The wall teichoic acids (WTA) in bacteria bind to the C6 of the N-acetylmuramic acid in peptidoglycan via a phosphate group in the linkage unit. Similar potential binding sites are found on the C6 of the N-acetyltalosaminuronic acid in pseudopeptidoglycan.

result of nucleation or passive deposition of nanometre-sized grains. Many cells were already coated in a relatively thick outer layer (Figure 6a,d) whereas others, including fimbriae, were somewhat embedded in a silica precipitate rather than coated. However, only the cells had precipitate coatings that covered the whole filament and reproduced the initial morphology. As with the phosphatic precipitates, the coating of cells was heterogeneous, with some covered in a full jacket (Figure 6a,d,e), others only partly coated (Figure 6c) and others completely uncoated, even at 3 months (Figure 6e). Gaboyer et al. (2017) noted similar tendencies in their experiments on the gram-negative bacterium *Yersinia* up to 6 months. Live/dead staining in their study indicated the presence of still-living cells able to resist encrustation by bacteria. In our experiments, some methanogens showed signs of lysis already at 2 weeks (Figure 5a) and 1 month (Figure 4g), but others remained turgid and whole well into 3 months (Figures 4e and 6e). Furthermore, Gaboyer et al. also observed silica precipitation in an amorphous phase only on the outside, never proceeding to the inside of the cells, something which also did not occur here. Previous experiments on the silicification of methanogens have demonstrated the possibility of silica precipitation on the inside of the cell as well, but these were carried out for up to a year (Orange et al. 2009).

TEM images reveal that the silica precipitation was not in direct contact with the cell wall but rather slightly removed from it (Figure 6f). This has previously been observed and was suggested as a possible repulsion effect of silica by the cell (Orange et al. 2009). Silica is formed as a colloidal precipitate due to the addition of sodium silicate in a buffered solution of pH 7.4 to a final supersaturated concentration. The silica therefore nucleates in solution, followed by the formation of an amorphous silica precipitate (Maryani et al. 2018). Protons on the surface of colloidal silica often dissociate into solution, leaving a high negative charge and where it comes into contact with the negatively charged cell wall, it is repelled. Phosphate anions, on the other hand, are more likely to nucleate directly on the surfaces of the cells due to the presence of calcium ions clustered around the cell wall that act as a bridge between the negatively charged surface of the cell and the phosphate (Orange et al. 2009; Kish et al. 2016). Considering the immediate formation of amorphous silica in solution, the cations do not act as nucleation sites. Precipitation of calcium silicate would, in any case, require a higher pH (10–12) (Ntafalias and Koutsoukos 2010). Furthermore, experiments with phosphate mineralising solution contain more calcium ions from the added calcium chloride than do silica experiments, where the only calcium is that present in the medium. Nevertheless, experiments with only methanogens and no added mineralising agent also produced calcium phosphates, possibly because of the cation bridge effect. The solubility of phosphate is lower than that of silicate, and at pH 7, phosphates can readily precipitate as calcium phosphate. There may also be another unknown mechanism with which methanogens remove phosphates from solution purposefully, since phosphorus has been shown to inhibit methanogenesis (Mancipe-Jiménez et al. 2017). This remains to be researched in the future. The presence of methanogen-shaped holes in some samples (Figure 7a,b) shows the close association between microbes and precipitate, a phenomenon previously noted between bacteria and calcite (Banks et al. 2010).

Several studies have noted that no significant differences could be discerned in the silica precipitation rate between samples containing methanogens (Orange et al. 2009) or bacteria (Yee et al. 2003) and sterile controls. In some cases, there may be a slight increase in rate with microbes or organic matter present, but that after the initial coating, the silicification proceeds abiotically (Benning et al. 2003; Orange et al. 2009). Evidently, at high silica concentration, there is such a strong drive for polymerisation, homogeneous nucleation, and precipitation that any effect of microbial catalysis is negligible. The *Methanobacterium* sp. strain used here resisted silicification for long enough to retain its morphology when it was eventually coated. Silicification was the most efficacious in forming uniform coatings around the methanogens, which can be particularly well seen in Figure 6c. The texture resembles that of silicified microbes in modern hot springs from New Zealand (Benning et al. 2005). The coating increases the overall diameter by a factor of >2 (Figure 6a) and ultimately even more, from 250 nm up to 1.4 μm (Figure 6e). This result may inform the interpretation of microbial fossils: a mineral filament with a diameter of more than 1 μm can be produced by an organism almost 6 times smaller. Fossil specimens of cyanobacteria have demonstrated this bias, where the increased diameter of the mineral leads to misidentification of the taxon (Peel 1988). Varying degrees of size are also present in the same group (Figure 6e) which could be interpreted as different species of microbes in a single colony, but here we show that the same microbe can create quite differently sized casts depending on the timing of initial mineral precipitation. The question remains whether or not the interior of the mineral coat better reflects the true size of the microbe. On measuring the size of cell cross-sections in TEM images, the diameter is often around 250 nm, in keeping with the cell size of the original methanogen. However, occasionally the diameter of the methanogen cross-section plus the halo of space created around it had a diameter of up to 450 nm. This occurred particularly commonly in the silica experiments (Figure 6f) but some phosphatised samples had a similar internal cavity of up to 350 nm. Were the cells to vanish and leave behind only a cavity or mould in the precipitate (Figure 7a,b), the diameter measured would falsely indicate a larger microorganism than a methanogen. TEM images that show a circular or oval-shaped halo can also be seen in similar experiments on the silicification of gram-negative bacteria (Westall 1997). In any case, most studies today do not rely solely on morphological characteristics as an indicator of microbial life. Detailed large- and small-scale analysis of the geological context of fossils is necessary (Javaux 2019) as well as the presence of concrete geochemical evidence of life-like isotopes (Lepot et al. 2013) or biomolecules (Alleon et al. 2019), among others.

Perhaps similar structures are found in natural microbialites where the initial stages of fossilization have been observed (Benning et al. 2005; Couradeau et al. 2013; Li et al. 2013). In ancient materials, phosphate minerals often occur with both carbonates and early diagenetic silica, but we are unaware of reports that closely match our experimental observations of individual mineralised microorganisms. In the future, fieldwork is necessary to ascertain whether or not the mineralisation processes in contemporary natural environments may unfold along similar lines to those seen in the experiments presented here. Further work to explore diagenetic/low-grade metamorphic alteration of the materials produced in our experiments would also be fruitful.

5 | Conclusion

This study investigated the precipitation of three common minerals found on earth: carbonate, phosphate, and silicate, on a methanogen strain with a novel cell wall structure. The results showed that silica in particular can precipitate in close association with the cell wall and that it creates a close-fitting coating of precipitate around the cells that increases preservation potential. However, the silica coating was more than three times the diameter of the original filament, and this taphonomic effect could mislead investigators. Care should be taken when interpreting silicified filamentous microfossils in the rock record, as their large size may be artefactual. Furthermore, depending on the stage of silicification, the methanogens had coatings of varying thickness throughout the different phases of mineralisation, with some remaining uncoated even at 3 months. If translated into the fossil record, this heterogeneity may create a misleading impression of morphological diversity in an originally monospecific population.

Experiments with phosphate precipitation showed a strong affinity between the methanogen species and phosphates. In all experiments, even those carried out in low-phosphate medium, phosphates formed on and around the methanogens. Often this was simply due to supersaturation, and the resulting precipitate was an amorphous precursor to apatite (Krajewski et al. 1994). However, in many samples, methanogens were closely coated with the phosphatic precipitate, and in particular the methanogens grown in low-phosphate medium with no mineralising agent added had phosphate precipitates that formed very near to the cell surfaces. We suggest that the negatively charged polymers found in the pseudomurein cell wall, in particular the hydroxyl binding sites for phosphate found in the N-acetyltalosaminuronic acid of the pseudomurein, act as nucleation sites for phosphate precipitation in addition to cations acting as bridges between the cell wall and anion. Further studies are needed to evaluate the role of methanogenic metabolites formed in solution in accordance with phosphate precipitation.

Acknowledgements

We thank Michael Streng (Uppsala University, UU) for assistance with SEM/EDX and Mikael Ottosson (UU) for XRD. Experiments were largely carried out at the Swedish University of Agricultural Sciences (SLU) with the assistance of Anna Schnürer and Simon Isaksson, whom we thank.

Conflicts of Interest

The authors declare no conflicts of interest.

Data Availability Statement

The data that support the findings of this study are available from the corresponding author upon reasonable request.

References

Alleon, J., D. T. Flannery, N. Ferralis, et al. 2019. "Organo-Mineral Associations in Chert of the 3.5 Ga Mount Ada Basalt Raise Questions About the Origin of Organic Matter in Paleoarchean Hydrothermally Influenced Sediments." *Scientific Reports* 9, no. 1: 16712.

Alleon, J., S. Bernard, C. Le Guillou, et al. 2016. "Early Entombment Within Silica Minimizes the Molecular Degradation of Microorganisms During Advanced Diagenesis." *Chemical Geology* 437: 98–108.

Araujo, J. C., F. C. Téran, R. A. Oliveira, et al. 2003. "Comparison of Hexamethyldisilazane and Critical Point Drying Treatments for SEM Analysis of Anaerobic Biofilms and Granular Sludge." *Journal of Electron Microscopy* 52, no. 4: 429–433.

Aylward, G. H., and T. J. V. Findlay. 1974. *SI Chemical Data*, 30. Wiley.

Banks, E. D., N. M. Taylor, J. Gulley, et al. 2010. "Bacterial Calcium Carbonate Precipitation in Cave Environments: A Function of Calcium Homeostasis." *Geomicrobiology Journal* 27, no. 5: 444–454.

Battistuzzi, F. U., A. Feijao, and S. B. Hedges. 2004. "A Genomic Timescale of Prokaryote Evolution: Insights Into the Origin of Methanogenesis, Phototrophy, and the Colonization of Land." *BMC Evolutionary Biology* 4: 1–14.

Benning, L. G., V. Phoenix, N. Yee, and K. O. Konhauser. 2003. "The Dynamics of Cyanobacterial Silicification: An Infrared Micro-Spectroscopic Investigation." *Geochimica et Cosmochimica Acta* 68: 743–757.

Benning, L. G., V. R. Phoenix, B. W. Mountain, and H. Lappin-Scott. 2005. "Biosilicification: The Role of Cyanobacteria in Silica Sinter Deposition." In *Symposia-Society for General Microbiology*, vol. 65, 131. Cambridge University Press.

Benzerara, K., N. Menguy, F. Guyot, et al. 2004. "Biologically Controlled Precipitation of Calcium Phosphate by *Ramlibacter tataouinensis*." *Earth and Planetary Science Letters* 228, no. 3: 439–449.

Beveridge, T. J., and R. G. Murray. 1980. "Sites of Metal Deposition in the Cell Wall of *Bacillus subtilis*." *Journal of Bacteriology* 141, no. 2: 876–887.

Bigi, A., E. Boanini, C. Capuccini, and M. Gazzano. 2007. "Strontium-Substituted Hydroxyapatite Nanocrystals." *Inorganica Chimica Acta* 360, no. 3: 1009–1016.

Boone, D. R. 2015. "*Methanobacterium*." In *Bergey's Manual of Systematics of Archaea and Bacteria*, 1–8. Wiley.

Brichni, A., H. Hammi, S. Aggoun, and A. Mnif. 2016. "Optimisation of Magnesium Oxychloride Cement Properties by Silica Glass." *Advances in Cement Research* 28, no. 10: 654–663.

Briggs, D. E. 2003. "The Role of Decay and Mineralization in the Preservation of Soft-Bodied Fossils." *Annual Review of Earth and Planetary Sciences* 31, no. 1: 275–301.

Burggraf, S., K. O. Stetter, P. Rouviere, and C. R. Woese. 1991. "*Methanopyrus kandleri*: An Archaeal Methanogen Unrelated to all Other Known Methanogens." *Systematic and Applied Microbiology* 14, no. 4: 346–351.

Cassier-Chauvat, C., and F. Chauvat. 2014. "Responses to Oxidative and Heavy Metal Stresses in Cyanobacteria: Recent Advances." *International Journal of Molecular Sciences* 16, no. 1: 871–886.

Cavalazzi, B., L. Lemelle, A. Simionovici, et al. 2021. "Cellular Remains in a~3.42-Billion-Year-Old Subseafloor Hydrothermal Environment." *Science Advances* 7, no. 29: eabf3963.

Cosmidis, J., and A. S. Templeton. 2016. "Self-Assembly of Biomorphic Carbon/Sulfur Microstructures in Sulfidic Environments." *Nature Communications* 7, no. 1: 12812.

Couradeau, E., K. Benzerara, E. Gérard, et al. 2013. "Cyanobacterial Calcification in Modern Microbialites at the Submicrometer Scale." *Biogeosciences* 10, no. 8: 5255–5266.

Curran, D. J., T. J. Fleming, M. R. Towler, and S. Hampshire. 2011. "Mechanical Parameters of Strontium Doped Hydroxyapatite Sintered

Using Microwave and Conventional Methods." *Journal of the Mechanical Behavior of Biomedical Materials* 4, no. 8: 2063–2073.

do Nascimento Vieira, A., K. Kleinermanns, W. F. Martin, and M. Preiner. 2020. "The Ambivalent Role of Water at the Origins of Life." *FEBS Letters* 594, no. 17: 2717–2733.

Esko, J. D., T. L. Doering, and C. R. Raetz. 2009. "Eubacteria and Archaea." In *Essentials of Glycobiology*, 2nd ed. Cold Spring Harbor Laboratory Press.

Ferris, F. G., W. S. Fyfe, and T. J. Beveridge. 1988. "Metallic Ion Binding by *Bacillus subtilis*; Implications for the Fossilization of Micro-Organisms." *Geology* 16: 149–152.

Francis, S., L. Margulis, and E. S. Barghoorn. 1978. "On the Experimental Silicification of Microorganisms II. On the Time of Appearance of Eukaryotic Organisms in the Fossil Record." *Precambrian Research* 6, no. 1: 65–100.

Frankel, R. B., and D. A. Bazylinski. 2003. "Biologically Induced Mineralization by Bacteria." *Reviews in Mineralogy and Geochemistry* 54, no. 1: 95–114.

Gaboyer, F., C. Le Milbeau, M. Bohmeier, et al. 2017. "Mineralization and Preservation of an Extremotolerant Bacterium Isolated From an Early Mars Analog Environment." *Scientific Reports* 7, no. 1: 8775.

Gunasekaran, S., G. Anbalagan, and S. Pandi. 2006. "Raman and Infrared Spectra of Carbonates of Calcite Structure." *Journal of Raman Spectroscopy* 37: 892–899.

Javaux, E. J. 2019. "Challenges in Evidencing the Earliest Traces of Life." *Nature* 572, no. 7770: 451–460.

Katsen-Globa, A., N. Puetz, M. M. Gepp, J. C. Neubauer, and H. Zimmermann. 2016. "Study of SEM Preparation Artefacts With Correlative Microscopy: Cell Shrinkage of Adherent Cells by HMDS-Drying." *Scanning* 38, no. 6: 625–633.

Keighley, D., S. Boonsue, and D. Hall. 2018. "Phosphatized Tungsten-Metabolizing Coccoid Microbes Interpreted From Oil Shale of an Eocene Lake, Green River Formation, Utah, USA." *Geobiology* 16: 610–627.

Kish, A., J. Miot, C. Lombard, et al. 2016. "Preservation of Archaeal Surface Layer Structure During Mineralization." *Scientific Reports* 6, no. 1: 26152.

Konhauser, K. O., B. Jones, V. R. Phoenix, G. Ferris, and R. W. Renaut. 2004. "The Microbial Role in Hot Spring Silicification." *Ambio* 33: 552–558.

Kontoyannis, C. G., and N. V. Vagenas. 2000. "Calcium Carbonate Phase Analysis Using XRD and FT-Raman Spectroscopy." *Analyst* 125, no. 2: 251–255.

Krajewski, K. P., P. V. Cappellen, J. Trichet, et al. 1994. "Biological Processes and Apatite Formation in Sedimentary Environments." *Eclogae Geologicae Helvetiae* 87: 701.

Lalonde, S. V., K. O. Konhauser, A. L. Reysenbach, and F. G. Ferris. 2005. "The Experimental Silicification of Aquificales and Their Role in Hot Spring Formation." *Geobiology* 3: 41–52.

Langerak, E. P. A. V., M. M. H. Beekmans, J. J. Beun, H. V. M. Hamelers, and G. Lettinga. 1999. "Influence of Phosphate and Iron on the Extent of Calcium Carbonate Precipitation During Anaerobic Digestion." *Journal of Chemical Technology & Biotechnology: International Research in Process, Environmental & Clean Technology* 74, no. 11: 1030–1036.

Lepot, K., K. H. Williford, T. Ushikubo, et al. 2013. "Texture-Specific Isotopic Compositions in 3.4 Gyr Old Organic Matter Support Selective Preservation in Cell-Like Structures." *Geochimica et Cosmochimica Acta* 112: 66–86.

Li, J., K. Benzerara, S. Bernard, and O. Beyssac. 2013. "The Link Between Biomineralisation and Fossilization of Bacteria: Insights From Field and Experimental Studies." *Chemical Geology* 359: 49–69.

Lucas, J., and L. Prévôt. 1985. "The Synthesis of Apatite by Bacterial Activity: Mechanism." *Sciences Geologiques, Memoire* 77: 83–92.

Ludwig, K. A., D. S. Kelley, D. A. Butterfield, B. K. Nelson, and G. Früh-Green. 2006. "Formation and Evolution of Carbonate Chimneys at the Lost City Hydrothermal Field." *Geochimica et Cosmochimica Acta* 70, no. 14: 3625–3645.

Mancipe-Jiménez, D. C., C. Costa, and M. C. Márquez. 2017. "Methanogenesis Inhibition by Phosphorus in Anaerobic Liquid Waste Treatment." *Waste Treatment and Recovery* 2, no. 1: 1–8.

Maryani, E., R. Septawendar, and S. Suhanda. 2018. "Effects of the Precipitation pH of Sodium Silicate on the Amorphous Silica Characteristics and Its Capability in the Pb and cd Adsorption." *Research Journal of Chemistry and Environment* 22: 172–178.

McMahon, S. 2019. "Earth's Earliest and Deepest Purported Fossils May Be Iron-Mineralized Chemical Gardens." *Proceedings of the Royal Society B* 286: 20192410.

Meyer, B. H., and S. V. Albers. 2020. *Archaeal Cell Walls*, 1–14. European Lisp Symposium.

Miot, J., S. Bernard, M. Bourreau, F. Guyot, and A. Kish. 2017. "Experimental Maturation of Archaea Encrusted by Fe-Phosphates." *Scientific Reports* 7: 16984.

Neubeck, A., L. Sun, B. Müller, et al. 2017. "Microbial Community Structure in a Serpentine-Hosted Abiotic Gas Seepage at the Chimaera Ophiolite, Turkey." *Applied and Environmental Microbiology* 83, no. 12: e03430.

Nims, C., J. Lafond, J. Alleon, A. S. Templeton, and J. Cosmidis. 2021. "Organic Biomorphs May Be Better Preserved Than Microorganisms in Early Earth Sediments." *Geology* 49, no. 6: 629–634.

Nitschke, W., S. E. McGlynn, E. J. Milner-White, and M. J. Russell. 2013. "On the Antiquity of Metalloenzymes and Their Substrates in Bioenergetics." *Biochimica et Biophysica Acta (BBA)-Bioenergetics* 1827, no. 8: 871–881.

Ntafalias, E., and P. G. Koutsoukos. 2010. "Spontaneous Precipitation of Calcium Silicate Hydrate in Aqueous Solutions." *Crystal Research and Technology: Journal of Experimental and Industrial Crystallography* 45, no. 1: 39–47.

Oehler, J. H. 1976. "Experimental Studies in Precambrian Paleontology: Structural and Chemical Changes in Blue-Green Algae During Simulated Fossilization in Synthetic Chert." *Geological Society of America Bulletin* 87, no. 1: 117–129.

Oehler, J. H., and J. W. Schopf. 1971. "Artificial Microfossils: Experimental Studies of Permineralization of Blue-Green Algae in Silica." *Science* 174, no. 4015: 1229–1231.

Orange, F., F. Westall, J. R. Disnar, et al. 2009. "Experimental Silicification of the Extremophilic Archaea Pyrococcus Abyssi and *Methanocaldococcus jannaschii*: Applications in the Search for Evidence of Life in Early Earth and Extraterrestrial Rocks." *Geobiology* 7, no. 4: 403–418.

Orange, F., J. R. Disnar, F. Westall, D. Prieur, and P. Baillif. 2011. "Metal Cation Binding by the Hyperthermophilic Microorganism, Archaea Methanocaldococcus Jannaschii, and Its Effects on Silicification." *Palaeontology* 54, no. 5: 953–964.

Passey, S., S. Pellegrin, and H. Mellor. 2007. "Scanning Electron Microscopy of Cell Surface Morphology." *Current Protocols in Cell Biology* 37, no. 1: 4–17.

Paula, F. S., J. P. Chin, A. Schnürer, et al. 2019. "The Potential for Polyphosphate Metabolism in Archaea and Anaerobic Polyphosphate Formation in *Methanosarcina mazei*." *Scientific Reports* 9, no. 1: 17101.

Peel, J. S. 1988. "Spirellus and Related Helically Coiled Microfossils (Cyanobacteria) From the Lower Cambrian of North Greenland." *Rapport. Grønlands Geologiske Undersøgelse* 137: 5–32.

Roberts, J. A., P. C. Bennett, L. A. González, G. L. Macpherson, and K. L. Milliken. 2004. "Microbial Precipitation of Dolomite in Methanogenic Groundwater." *Geology* 32, no. 4: 277–280.

Schieber, J., Y. Zawar, and M. Glamoclija. 2008. "Experiments on Silicification of Iron Microbes–A Preliminary Report." In 39th Annual Lunar and Planetary Science Conference (No. 1391, p. 2132).

Schnürer, A., F. P. Houwen, and B. H. Svensson. 1994. "Mesophilic Syntrophic Acetate Oxidation During Methane Formation by a Triculture at High Ammonium Concentration." *Archives of Microbiology* 162: 70–74.

Schultze-Lam, S., D. Fortin, B. S. Davis, and T. J. Beveridge. 1996. "Mineralization of Bacterial Surfaces." *Chemical Geology* 132, no. 1–4: 171–181.

Stephens, A. 2023. "*Methanobacterium* Cauma sp. nov. a Hydrogenotrophic, Halotolerant Methanogen from an Active Serpentinization System at Chimaera Seep." Master thesis. University of Uppsala and Swedish University of Agricultural Sciences.

Swoboda, J. G., J. Campbell, T. C. Meredith, and S. Walker. 2010. "Wall Teichoic Acid Function, Biosynthesis, and Inhibition." *Chembiochem: A European Journal of Chemical Biology* 11, no. 1: 35–45.

Thoma, C., M. Frank, R. Rachel, et al. 2008. "The Mth60 Fimbriae of Methanothermobacter Thermoautotrophicus Are Functional Adhesins." *Environmental Microbiology* 10, no. 10: 2785–2795.

Trewin, N. H., and A. H. Knoll. 1999. "Preservation of Devonian Chemotrophic Filamentous Bacteria in Calcite Veins." *PALAIOS* 14, no. 3: 288–294. https://doi.org/10.2307/3515441.

Ueno, Y., K. Yamada, N. Yoshida, S. Maruyama, and Y. Isozaki. 2006. "Evidence From Fluid Inclusions for Microbial Methanogenesis in the Early Archaean Era." *Nature* 440, no. 7083: 516–519.

Visscher, P. T., and J. F. Stolz. 2005. "Microbial Mats as Bioreactors: Populations, Processes, and Products." In *Geobiology: Objectives, Concepts, Perspectives*, 87–100. Elsevier.

Westall, F. 1997. "Influence of Cell Wall Composition on the Fossilisation of Bacteria and the Implications for the Search for Early Life Forms." In IAU Colloq. 161: Astronomical and Biochemical Origins and the Search for Life in the Universe (p. 491).

Yee, N., V. R. Phoenix, K. O. Konhauser, L. G. Benning, and F. G. Ferris. 2003. "The Effect of Cyanobacteria on Silica Precipitation at Neutral pH: Implications for Bacterial Silicification in Geothermal Hot Springs." *Chemical Geology* 199, no. 1–2: 83–90.

Zehnder, A. J., B. A. Huser, T. D. Brock, and K. Wuhrmann. 1980. "Characterization of an Acetate-Decarboxylating, Non-Hydrogen-Oxidizing Methane Bacterium." *Archives of Microbiology* 124: 1–11.

Supporting Information

Additional supporting information can be found online in the Supporting Information section.